

# Better Together: Joint Reasoning for Non-rigid 3D Reconstruction with Specularities and Shading

Qi Liu-Yin\* · Rui Yu\* · Lourdes Agapito · Andrew Fitzgibbon · Chris Russell

Received: date / Accepted: date

**Abstract** We demonstrate the use of shape-from-shading (sfs) to improve both the quality and the robustness of 3D reconstruction of dynamic objects captured by a single camera. Unlike previous approaches that made use of sfs as a post-processing step, we offer a principled integrated approach that solves dynamic object tracking and reconstruction and sfs as a single unified cost function. Moving beyond Lambertian sfs, we propose a general approach that models both specularities and shading while simultaneously tracking and reconstructing general dynamic objects. Solving these problems jointly prevents the kinds of tracking failures which can not be recovered from by pipeline approaches. We show state-of-the-art results both qualitatively and quantitatively.

**Keywords** Non-Rigid Structure from Motion · Shape from Shading · Non-Rigid Tracking

## 1 Introduction

As the quality of 3D reconstructions of dynamic and deformable objects such as animals and faces has improved,

\* The first two authors contribute equally.

Qi Liu-Yin · Rui Yu · Lourdes Agapito  
University College London, London, UK  
E-mail: {Qi.Liu,R.Yu,L.Agapito}@cs.ucl.ac.uk

Andrew Fitzgibbon  
Microsoft Research Cambridge, Cambridge, UK  
E-mail: awf@microsoft.com

Chris Russell  
University of Surrey  
and  
Alan Turing Institute, London, UK  
E-mail: cr0040@surrey.ac.uk

robustness and the reconstruction of semantically meaningful details like smile and frown lines become more important. These transient fine details can not be recovered by tracking alone, and require an understanding of the lighting in the environment and a knowledge of how the surface normals of the object affect its illumination.

While these shading artifacts can inform highly-detailed reconstructions, they can also prevent the tracking of objects. In homogeneously textured regions, such as human skin, the variance in the appearance of a patch due to lighting changes can be much greater than the difference in appearance between one patch and the next. A combination of these effects makes it vital that we model illumination changes if we wish to correctly capture facial deformations particularly those of the brow and cheeks.

The instability of color as a tracking cue is well known and much remarked upon in the literature. Focusing on recent works in dynamic 3D reconstruction using depth or multi-camera capture, it is noticeable how papers such as Dou et al. (2015); Newcombe et al. (2015) make use of raw depth maps without color information in reconstruction. Similarly, although the RGB-D based work Zollhofer et al. (2014) made use of color information they only matched appearance between pairs of adjacent frames as over long sequences changes in shadow and illumination made color matching unreliable. These problems can largely be ignored in the reconstruction of rigid scenes that do not move relative to the lighting environment. Here shading artifacts remain constant throughout the sequence, while specularities typically occur sparsely and can be handled without being explicitly modeled through the use of robust statistics (Newcombe et al., 2011).

In the field of non-rigid monocular reconstruction from RGB video, we are not so fortunate. With only a single RGB camera as input, we must make use of color information. However, without depth information, matching color only between pairs of frames is prone to drift, with many

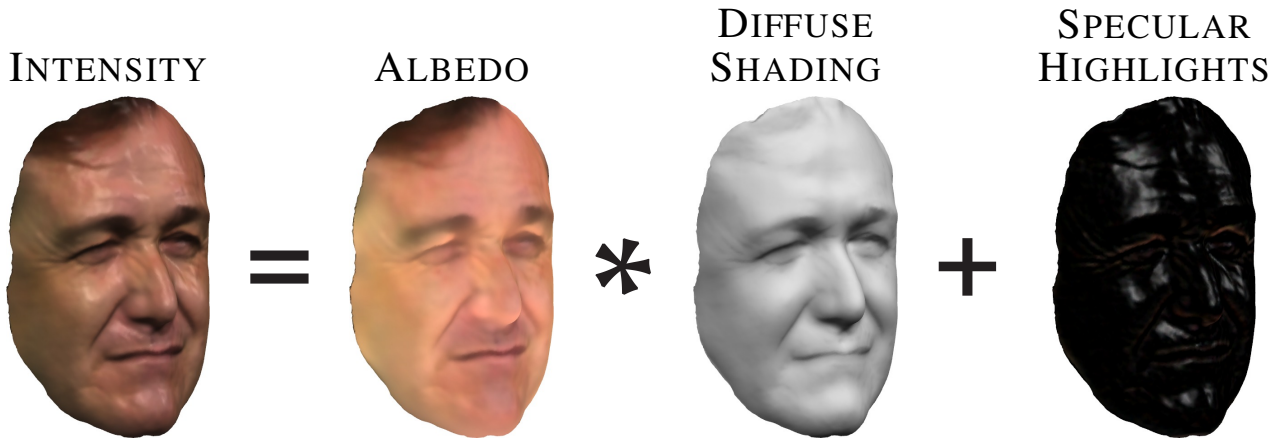


**Fig. 1** Intensity decomposition into the product of albedo and diffuse shading (as a function of spherical harmonics and 3D shape estimation) plus the specular component.

tracks gradually diffusing away from an object over long sequences (Sundaram et al., 2010). Similarly, moving objects can no longer be assumed to be static with respect to the lighting environment, and outside of a controlled studio-lit environment, changes in the orientation of objects lead to significant changes in appearance. Such changes often lead to the failure of direct image intensity based trackers such as Yu et al. (2015).

Building from cutting edge approaches to non-rigid monocular reconstruction from RGB video and *sfs*, we propose a unified framework for jointly reasoning about shape-from-shading and reconstructing arbitrary deforming objects. Unlike existing methods, our general approach is not object specific and targets non-Lambertian surfaces such as skin while modeling both specularities and shading. The importance of a unified framework becomes even more apparent when handling video shot outside the controlled lighting of a studio, where small rotations of an object can induce significant changes of appearance across most of the object, leading to a loss of tracking. Further, we empirically demonstrate that modeling the non-Lambertian properties of surfaces such as skin, and capturing both specularities and shading is vital for the joint integration of *sfs* with non-rigid reconstruction.

One of the main challenges in non-rigid 3D reconstruction lies in evaluating the quality of reconstructions. It is particularly challenging to capture dense deforming objects of interest with sufficiently high fidelity under real world lighting conditions. For example, depth data from an infra-red structured light source. e.g. the Microsoft Kinect or the purpose built depth camera of Zollhofer et al. (2014), can not be captured under strong natural light, while multi-camera visible-light techniques such as Valgaerts et al. (2012) require relatively uniform lighting to maintain tracking. To validate our approach we compare both on real world se-

quences captured using the stereo setup of Valgaerts et al. (2012), and use this data to generate realistic synthetic sequences containing severe shading artifacts that could not be tracked by Valgaerts et al. (2012). Our method displays a strong qualitative and quantitative improvement over these previous methods. See figure 2 and section 8.1 for details. Our code and new ground truth datasets for evaluation have been made publicly available.

## 2 Related Work

All previous attempts to unify shape-from-shading with non-rigid 3D reconstruction from RGB video have been pipeline approaches (Suwajanakorn et al., 2014; Malti et al., 2012; Valgaerts et al., 2012; Garrido et al., 2013) which first coarsely reconstruct these deformable objects and then apply shape-from-shading to refine the initial reconstruction. Examples of this include, the seminal work Face Reconstruction in the Wild (Kemelmacher-Shlizerman and Seitz, 2011), which first made use of automatic point correspondences to compute warps and align images of a variety of celebrities, before reconstructing faces using *sfs* to build dense face models. This was followed by Suwajanakorn et al. (2014), which refined a coarser intensity based model using *sfs*.

Varol et al. (2012) fused shape-from-shading with non-rigid reconstruction, but only performed shape-from-shading on untextured regions of the objects, and non-rigid reconstruction on the textured areas, before fusing these reconstructions as a post-processing step. Moreover, they required a known light field and could not reconstruct high-frequency details such as facial creases.

Several works have made use of *sfs* in refining depth maps, either captured directly using a depth scanner (Or El et al., 2015; El et al., 2016; Yu et al., 2013) or captured using

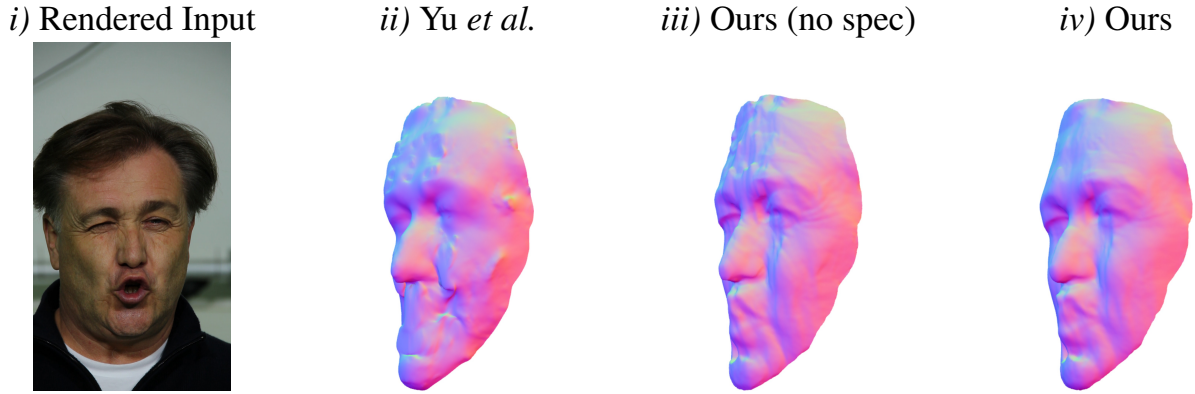


**Fig. 2** An illustration of our, and previous, approaches on a synthetic face sequence of a specular object under variable lighting. From Left to right: *i)* Sample frame *ii)* The direct reconstruction of Yu et al. (2015), that does not consider shading artifacts. *iii)* Our new approach that integrates sfs with non-rigid reconstruction but does not consider specularities. *iv)* Our unified framework for sfs, non-rigid structure from motion, and specular modeling. This framework improves the accuracy of our approach over Yu et al. by a factor of nearly 240% reducing the RMS error from 9.28mm to 3.84mm. Use of joint refinement rather than alternating refinement reduces the error further to 3.01mm and additional depth data almost halves the remaining error to 1.77mm. See discussion in section 8.1, and table 1 for details.

a multi-camera setup (Valgaerts et al., 2012). Of the RGB-D approaches El et al. (2016) is the most related to ours, and computes both sfs and specularities in order to enhance their depth maps. Previous works have also used sfs to improve tracking: In the multi-camera work of Beeler et al. (2012), they used a pipeline approach to improve the tracking and refine the shape of an initial reconstruction by both estimating and removing ambient occlusions. While Xu and Roy-Chowdhury (2005) defined linear equations for modeling changes of illumination and position that occur when tracking a rigid object in video.

Our work builds on the recent template-based approach to monocular and direct non-rigid 3D reconstruction of Yu et al. (2015). This work made no use of sfs, but generated vivid reconstructions of objects by deforming a known template to match direct photometric cost. We extend this direct formulation by augmenting the direct photometric cost with terms that capture the change in appearance that goes with shape and shading, leading to more lifelike and plausible reconstructions.

### 3 Problem Formulation

Consider a single RGB perspective camera, of known internal calibration, observing a non-rigid object. We propose a sequential, frame-by-frame, approach to capture both the 3D geometry and the reflectance properties of the non-rigid object. We parameterize the object at time-step  $t$  as a mesh  $\mathbf{S}^t$  with  $N$  vertices with associated 3D coordinates  $\mathbf{S}^t = \{\mathbf{s}_i^t\}$ ,  $i = 1..N$ .

Our proposed approach is summarized in Algorithm 1. The goal for each incoming frame at time  $t$  is to estimate the current 3D coordinates of the vertices of the mesh, the light field – parameterized in terms of spherical harmonics – and

---

#### Algorithm 1: Joint non-rigid 3D reconstruction and shape-from-shading

---

**Input** : 3D Template mesh  $\widehat{\mathbf{S}}$  + template albedo  $\widehat{\rho}_i$  (obtained using Algorithm 2)

Current video frame  $\mathbf{I}^t$

Solution to previous frame

$\{\mathbf{S}^{t-1}, \mathbf{R}^{t-1}, \mathbf{t}^{t-1}, \mathbf{I}^{t-1}, \beta^{t-1}\}$

**Output**: Deformed shape  $\mathbf{S}^t$ , rotation  $\mathbf{R}^t$ , translation  $\mathbf{t}^t$ ,

spherical harmonic coefficients  $\mathbf{I}^t$  and specularities  $\beta^t$

for current frame  $t$

1 **for** each new image frame  $\mathbf{I}^t$  **do**

2     **Initialize**  $\{\mathbf{S}^t, \mathbf{R}^t, \mathbf{t}^t, \mathbf{I}^t, \beta^t\} \leftarrow \{\mathbf{S}^{t-1}, \mathbf{R}^{t-1}, \mathbf{t}^{t-1}, \mathbf{I}^{t-1}, \beta^{t-1}\}$

3     Minimize (5) w.r.t. rigid alignment  $\{\mathbf{R}^t, \mathbf{t}^t\}$  holding  $\{\mathbf{S}^t, \mathbf{I}^t, \beta^t\}$  constant

4     Minimize (5) w.r.t. deformations and lighting  $\{\mathbf{S}^t, \mathbf{I}^t\}$  holding  $\{\mathbf{R}^t, \mathbf{t}^t, \beta^t\}$  constant

5     Minimize (5) w.r.t. specularities  $\beta^t$  holding  $\{\mathbf{S}^t, \mathbf{I}^t, \mathbf{R}^t, \mathbf{t}^t\}$  constant

6     **Joint refinement** Minimize (5) w.r.t. all variables:  $\mathbf{R}^t, \mathbf{t}^t, \mathbf{S}^t, \mathbf{I}^t$  and  $\beta^t$ .

7 **end**

---

specularities, as well as the overall rigid rotation and translation ( $\mathbf{R}^t, \mathbf{t}^t$ ) that align the deformed shape and a reference 3D template. The only inputs to our method are: the current image frame  $\mathbf{I}^t$ , the solution to the previous frame, and a 3D template of the object (including its geometry  $\widehat{\mathbf{S}}$  and albedo map  $\widehat{\rho}_i$ ) acquired in a preliminary stage described in Section 7 and Algorithm 2. Note that all variables related to the template are denoted with  $\widehat{\cdot}$ .

### 4 Reflectance Model

Modern solutions, such as Yu et al. (2015); Suwajanakorn et al. (2014); Valgaerts et al. (2012), to *direct* 3D reconstruc-

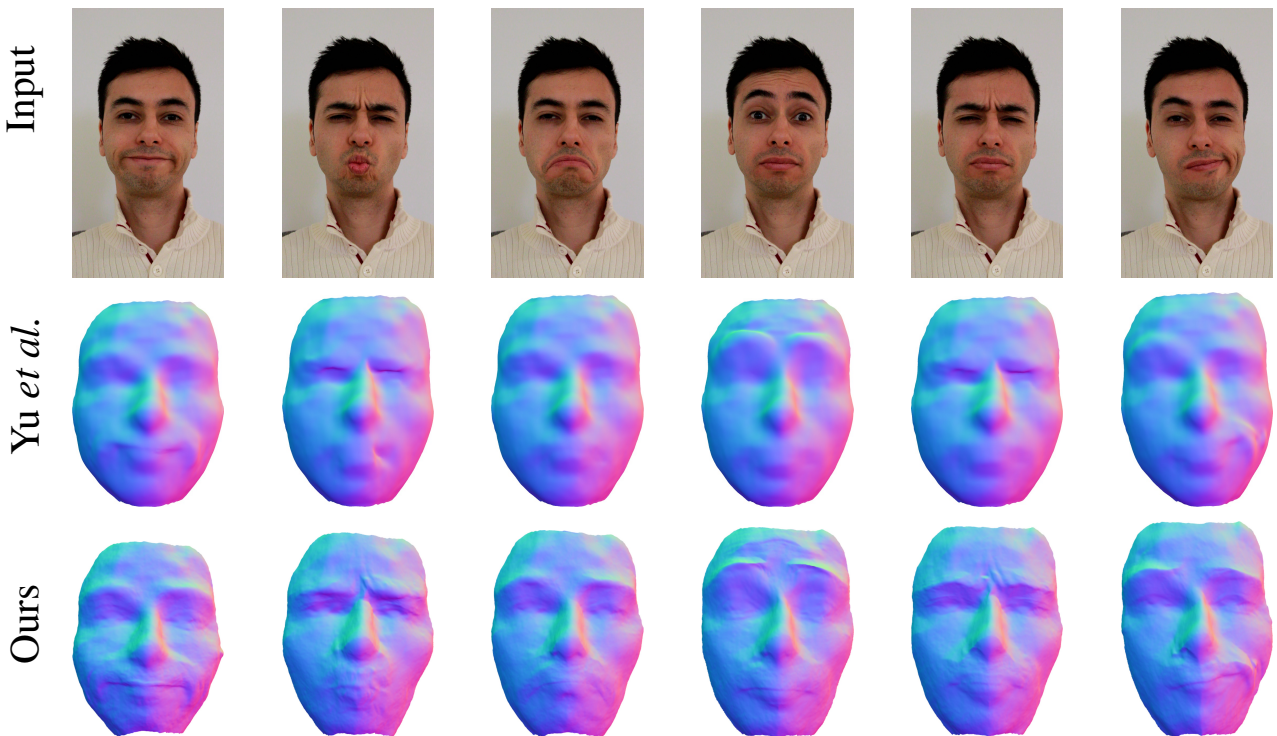


Fig. 3 Best viewed in color: A qualitative comparison of our method against that of Yu et al. (2015), on their face dataset.

tion of non-rigid objects from RGB video adopt an energy optimization approach that minimizes a robust photometric cost based upon *brightness constancy*. In other words, they jointly estimate dense correspondences alongside non-rigid deformations, by penalizing differences in intensity between images and the new deformed shape, which is assumed to be the same color and brightness of a reference template. As the points on the object change color in response to differences in illumination or in shading caused by strong deformations these methods need to use robust costs to cope with deviations from the model.

In contrast, our method explicitly models the reflectance properties of non-Lambertian objects and can handle materials which exhibit a mixture of specular and diffuse reflection properties. In practice we adopt an approximation of the Phong reflection model which models light leaving the non-rigid object at point  $i$  as the sum of two additive terms: a viewpoint-independent diffuse term and a view-dependent specular term:

$$\mathbf{I}_i = \mathbf{I}_i^{\text{diff}} + \beta_i. \quad (1)$$

In other words, the intensity at point  $i$  can be explained as the sum of the specularity-free diffuse component  $\mathbf{I}_i^{\text{diff}}$  and the specular component  $\beta_i$ .

To increase our robustness to changes in lighting and shading and to recover high frequency details of the object geometry, we decouple the diffuse component into the product of object albedo and the object irradiance or shading (see

figure 1). While the albedo is independent of the surface orientation, the shading is a function of the surface normal at each vertex  $i$

$$\mathbf{I}_i^{\text{diff}} = \rho_i r(\mathbf{n}_i(\mathbf{S})). \quad (2)$$

Here  $\rho_i$  is the RGB reflectance or albedo,  $\mathbf{n}_i(\cdot)$  is a function that returns the direction of the surface normal at vertex  $i$ , and  $r(\cdot)$  is an irradiance map function that returns the shading value given the surface orientation vector. We assume white illumination so  $r(\cdot)$  returns a single scalar value greater than 0.

Following Basri and Jacobs Basri and Jacobs (2003) we model the irradiance map using a spherical harmonic basis

$$r(\mathbf{n}_i(\mathbf{S})) = \sum_{n=0}^N \sum_{m=-n}^n l_{nm} Y_{nm}(\mathbf{n}_i(\mathbf{S})) = \mathbf{l} \cdot \mathbf{Y}(\mathbf{n}_i(\mathbf{S})) \quad (3)$$

where  $l_{nm}$  is the coefficient associated with the spherical harmonic function  $Y_{nm}$ . We limit our approximation to second order spherical harmonics, i.e.  $N = 2$  giving 1 nine coefficients.

If we consider a video of a non-rigid object evolving over time  $\mathbf{S}^t$ , our reflection model allows us to write the predicted image intensity of point  $i$  observed at time  $t$  as

$$\mathbf{I}_i^t = \rho_i \mathbf{l}^t \cdot \mathbf{Y}(\mathbf{n}_i(\mathbf{S}^t)) + \beta_i^t \quad (4)$$

It is clear that our reflection model allows us to cope not only with varying geometry ( $\mathbf{S}^t$ ) but also varying illumination coefficients ( $\mathbf{l}^t$ ) and specularities ( $\beta_i^t$ ). Notably, while

the image brightness of vertex  $i$  might vary over time  $t$  due to possible changes in illumination and object surface normals  $\mathbf{n}_i(\mathbf{S}^t)$  caused by the deformations, its albedo  $\rho_i$  is constant over the entire sequence.

While previous approaches to non-rigid object reconstruction from RGB video might include a post-processing step to add high frequency details to the tracked objects by performing a similar shape-from-shading decomposition Suwajanakorn et al. (2014) our work incorporates this step directly into the 3D tracking. In essence, our approach effectively takes advantage of changes in shading caused by variations in the illumination and in the surface normals due to deformations to improve 3D tracking while recovering high frequency surface details.

Previous approaches based on *brightness constancy* needed to adopt robust penalty terms to be able to discard specularities as outliers or to be resilient to changes to illumination. We will show that the benefits of modeling these effects directly in our reflectance model are twofold: (i) substantial improvements in 3D non-rigid tracking and (ii) direct recovery of high frequency geometry details such as folds and wrinkles.

Our insight and the main contribution of this work is to track the non-rigid deformations of the object based on *albedo constancy* instead of the more classical *image brightness constancy* constraint which does not hold for non-rigid objects or when the illumination varies over time. In this way, we can take advantage of the changes in illumination and shading to recover high frequency details in non-rigid objects and by increasing 3D tracking accuracy.

## 5 A Sequential Approach to Joint Non-Rigid 3D Reconstruction and Reflectance Estimation

Much like Yu et al. (2015), we use a template-based approach to track and reconstruct non-rigid objects. However, while Yu et al. (2015) assigned a fixed intensity to each vertex on the template mesh, we decompose the intensity of each vertex (see equation (4)) allowing us to take advantage of the reflectance properties of the object to improve the resulting reconstructions.

### 5.1 Our Energy

Our per-frame objective takes the form

$$E(\mathbf{S}, \mathbf{R}, \mathbf{t}, \mathbf{l}, \boldsymbol{\beta}) = E_{\text{data}}(\mathbf{S}, \mathbf{R}, \mathbf{t}, \mathbf{l}, \boldsymbol{\beta}) + E_{\text{smooth}}(\mathbf{S}, \boldsymbol{\beta}) \quad (5)$$

$$+ E_{\text{arap}}(\mathbf{S}) + E_{\text{temp}}(\mathbf{S}, \mathbf{t}, \mathbf{l}, \boldsymbol{\beta})$$

$$+ E_{\text{sparse}}(\boldsymbol{\beta})$$

#### 5.1.1 Data Term $E_{\text{data}}$ :

Our data term is a direct photometric cost. Rather than minimizing the more commonly used *brightness constancy constraint* we use the more complex reflectance model described in (4) which decomposes the intensity of vertex  $i$  into the product of a constant albedo and a time-varying shading term (where variations can be due to changes in illumination or to strong deformations) and explicitly models specularities.

$$E_{\text{data}}(\mathbf{R}, \mathbf{t}, \mathbf{S}, \mathbf{l}, \boldsymbol{\beta}) = \sum_{i \in \mathcal{V}} \left\| \mathbf{I}(\pi(\mathbf{R}(\mathbf{s}_i) + \mathbf{t})) - \hat{\rho}_i \mathbf{l} \cdot Y(\mathbf{R}(\mathbf{n}_i(\mathbf{S}))) - \beta_i \right\|_{\epsilon} \quad (6)$$

where  $\mathbf{I}$  is the current image frame,  $\mathcal{V}$  is the set of estimated visible vertices,  ${}^1 \mathbf{R}$  and  $\mathbf{t}$  are the rigid rotation and translation of the object,  $\{\mathbf{s}_i\}_1^N$  are the 3D vertices of the shape in the current frame,  $\pi(\cdot)$  is the projection from 3D points to image coordinates, known from camera calibration, and  $\hat{\rho}_i$  is the albedo of vertex  $i$  on the template mesh. and  $\|\cdot\|_{\epsilon}$  is the Huber loss.

#### 5.1.2 Spatial Smoothness Term $E_{\text{smooth}}$ :

This regularization term encourages spatially smooth deformations of the shape and specularities. In practice the spatial smoothness on the shape is decoupled into two terms: a total variation term that encourages smooth deformations of the shape  $\mathbf{S}$  with respect to the template  $\hat{\mathbf{S}}$  and a *Laplacian* smoothness term

$$E_{\text{smooth}}(\mathbf{S}, \boldsymbol{\beta}) = E_{\text{smooth}}(\mathbf{S}) + E_{\text{smooth}}(\boldsymbol{\beta}) \quad (7)$$

$$= E_{\text{TV}}(\mathbf{S}) + E_{\text{Laplacian}}(\mathbf{S}) + E_{\text{spec}}(\boldsymbol{\beta})$$

$$= \sum_{i \in \mathcal{V}} \sum_{j \in \mathcal{N}_i} \|(\mathbf{s}_i - \mathbf{s}_j) - (\hat{\mathbf{s}}_i - \hat{\mathbf{s}}_j)\|_{\epsilon}$$

$$+ \sum_{i \in \mathcal{V}} \frac{1}{|\mathcal{N}_i|} \left\| \sum_{j \in \mathcal{N}_i} (\mathbf{s}_i - \mathbf{s}_j) \right\|_2^2$$

$$+ \sum_{i \in \mathcal{V}} \sum_{j \in \mathcal{N}_i} \|\beta_i - \beta_j\|_{\epsilon}$$

where  $\mathcal{N}_i$  is the neighborhood of  $i$ .

#### 5.1.3 ARAP Term $E_{\text{arap}}$ :

This *as rigid as possible* cost (Sorkine and Alexa, 2007) encourages non-rigid objects to preserve locally rigidity while

<sup>1</sup> This is generated by realigning the deformed mesh of the previous frame to minimize photometric error, and z-buffering.

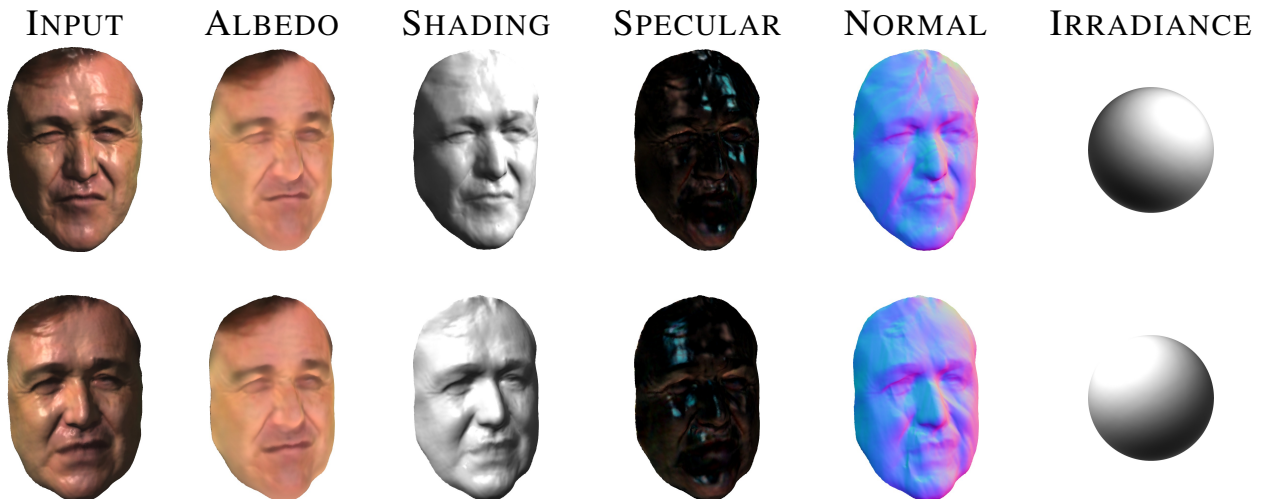


**Fig. 4** Results of two different frames from the synthetic SC sequence (see section 8.1) and the corresponding intrinsic decomposition (section 4).

deforming. It allows for local rotations to occur while preserving the relative locations between neighboring points.

$$E_{\text{arap}}(\mathbf{S}, \{\mathbf{A}_i\}) = \sum_{i=1}^N \sum_{j \in \mathcal{N}_i} \|(\mathbf{s}_i - \mathbf{s}_j) - \mathbf{A}_i(\widehat{\mathbf{s}}_i - \widehat{\mathbf{s}}_j)\|_2^2 \quad (8)$$

where the variables  $\mathbf{A}_i$  describe per-point local rotations.

#### 5.1.4 Temporal Smoothness $E_{\text{temp}}$ :

This set of temporal regularizers prevents flickering throughout the sequence

$$E_{\text{temp}}(\mathbf{S}, \mathbf{t}, \mathbf{l}, \boldsymbol{\beta}_i) = \|\mathbf{S} - \mathbf{S}^{t-1}\|_{\mathcal{F}}^2 + \|\mathbf{t} - \mathbf{t}^{t-1}\|_2^2 + \|\mathbf{l} - \mathbf{l}^{t-1}\|_2^2 + \|\boldsymbol{\beta} - \boldsymbol{\beta}^{t-1}\|_2^2 \quad (9)$$

where  $\mathbf{S}^{t-1}$ ,  $\mathbf{t}^{t-1}$ ,  $\mathbf{l}^{t-1}$ ,  $\boldsymbol{\beta}^{t-1}$  are the shape, translation, spherical harmonic coefficients and specularities in the previous frame and  $\|\cdot\|_{\mathcal{F}}$  denotes the Frobenius norm of a matrix.

#### 5.1.5 Sparsity Term $E_{\text{sparse}}$ :

This prevents the entire image being “explained away” as a specularity, by penalizing the use of specularities.

$$E_{\text{sparse}}(\boldsymbol{\beta}) = \sum_{i \in \mathcal{V}} \|\boldsymbol{\beta}_i\|_{\epsilon} \quad (10)$$

#### 5.1.6 Energy Optimization:

For reasons of efficiency, we adopt a multi-stage optimization similar to the approach taken by real-time SLAM approaches such as Klein and Murray (2007). Starting from the solution given by the previous frame, we hold all other coefficients fixed and optimize first over rotations and translations, followed by jointly optimizing shape and spherical

harmonic coefficients, and finally re-estimating the specularities.

The first two of these optimizations are performed coarse-to-fine over a 3-layer spatial pyramid, providing robustness against sudden movements and deformations of the object while for efficiency reasons, specularities are only estimated at the finest level, and propagated to the coarser levels of the pyramid, ready for the next iteration. Algorithm 1 summarizes our optimization strategy. We use the Levenberg-Marquardt implementation from the Ceres solver (Agarwal et al., 2012) for all continuous optimization, applying preconditioned conjugate gradient for the linear solver. When handling color images, the pyramid is formed by down-sampling using Gaussian filters, while for depth images a median filter is used to avoid artifacts along the boundary of the object.

In the experimental section, particularly table 1, we also compare against performing joint optimization over all variables to convergence, after initializing each frame using the procedure described above. This leads to a noticeable improvement in performance.

## 6 Reconstructing with RGB-D data

We also consider sequences where depth cues have been provided by an RGB-D camera such as the Microsoft Kinect (Newcombe et al., 2015), or an Infra-red stereo setup (Zollhofer et al., 2014). Even with powerful depth cues, visual tracking provides important information that allows the correct tracking of smooth and deforming surfaces such as the cheeks and brow of a person. As previously discussed these color cues can be polluted by shading effects, making tracking based purely on color consistency and depth challenging. Moreover, these shading cues provide important information about the high-frequency changes in depth such as

**Algorithm 2:** 3D Template acquisition

- 
- Input** : Rigid image subsequence  $\{\mathbf{I}_{\text{rigid}}^f\}_{f=1, \dots, F}$   
**Output**: 3D coordinates of template mesh vertices  $\hat{\mathbf{S}} = \{\hat{\mathbf{S}}_i\}$   
 and  
 Template albedo map  $\hat{\rho} = \{\hat{\rho}_i\}$  where  $i = 1 \dots N$
- 1 Obtain rigid camera poses for each frame  $\{\mathbf{I}_{\text{rigid}}^f\}$  using VisualSFM Wu (2011)
  - 2 Estimate 3D template mesh vertices  $\hat{\mathbf{S}} = \{\hat{\mathbf{s}}_i^f\}$  using MVS Campbell et al. (2008); Vogiatzis et al. (2007); Hernández et al. (2007)
  - 3 Estimate diffuse component  $\hat{\mathbf{I}}_i^{\text{diff}} \forall i$  template vertices as median color over all frames
  - 4 Solve for the illumination coefficients  $\hat{\mathbf{I}}$  minimizing (12) assuming white albedo
  - 5 Solve for albedo map of the template  $\hat{\rho} = \{\hat{\rho}_i\}$  minimizing (13)
- 

creases about the brow and eyes that are too fine to be captured directly by depth sensors.

As such, it is vital to make use of the entire pipeline we have proposed as well as depth cues for vivid high-quality reconstructions that are robust to the effects of lighting. In these cases, the energy can be augmented by an additional term that encourages consistency between the depth map and the generated reconstruction. In this case, we introduce an additional cost based on the distance between the reconstruction and the depth map

$$E_{\text{depth}}(\mathbf{S}, \mathbf{D}) = \sum_{i=1}^N \arg \min_{\mathbf{d} \in \mathbf{D}} \|\mathbf{s}_i - \mathbf{d}\|_{\epsilon} \quad (11)$$

Qualitatively improved results from using depth, and a comparison against the method of Zollhofer et al. (2014), which only makes use of frame-to-frame color based tracking, rather than a SfM model can be seen in figure 5. The strong illumination effects of this sequence prevent us from a direct comparison with any method such as Yu et al. (2015) that makes use of sequence based color consistency. More details about the experimental setup are given in section 8.2. With no better method available (all methods make use of RGB-D) data, a quantitative comparison between Zollhofer et al. (2014) and our work is not possible. However, section 8.2 discusses how depth images can improve our reconstructions on synthetic sequences against a known ground-truth.

## 7 Template Capture

This section describes how we capture the static geometry and the reflectance properties of the object of interest – or in other words how we build the template model used for tracking. We achieve this by moving a hand-held camera around the object while it remains rigid for a few seconds, to observe it from different angles. During the template capture step, we assume that the illumination remains constant.

### Template geometry:

For each frame we estimate the relative pose of the camera with respect to the object using a standard off-the-shelf structure from motion approach (VisualSFM Wu (2011)). We then use the multi-view stereo approach of Campbell et al. (2008) to produce individual depth maps for each frame. Finally the depth maps are fused using the volumetric technique of Vogiatzis et al. (2007) and the probabilistic visibility approach of Hernández et al. (2007) to produce as output a watertight mesh of the template shape parameterized as the set of 3D vertex coordinates  $\hat{\mathbf{S}} = \{\hat{\mathbf{s}}_i\}, i = 1..N$ .

### Template reflectance properties:

The next step of the template acquisition stage is to assign a color value to each vertex  $i$  on the mesh. Our implicit assumption is that the light leaving the surface of the template is the sum of a viewpoint-independent diffuse term and a view-dependent specular term. We estimate the diffuse term  $\hat{\mathbf{I}}_i^{\text{diff}}$  as the median color over all the frames in the rigid subsequence in which the projected vertex is visible. While some previous approaches favored the use of the minimum observed intensity value (Nishino et al., 2001), we choose to use the median as proposed by Wood et al. (2000) (also used in the color template generation of Yu et al. (2015)) since it provides robustness to shadows and errors in the camera tracking.

We decompose the diffuse component of the template  $\hat{\mathbf{I}}_i^{\text{diff}}$  further into the product of an *albedo map* and an irradiance function parameterized in terms of *spherical harmonics* to approximate the illumination and the surface normals as described in (4). First we solve for the *spherical harmonic coefficients* by optimizing the following photometric objective function with respect to  $\hat{\mathbf{I}}$ :

$$E_{\text{template}}(\hat{\mathbf{I}}) = \sum_{i \in \mathcal{V}} \left\| \hat{\mathbf{I}}_i^{\text{diff}} - \hat{\rho}_i \mathbf{1} \cdot Y(\mathbf{n}_i(\hat{\mathbf{S}})) \right\|_{\epsilon} \quad (12)$$

where  $\hat{\rho}_i$  is an initial assumption of the albedo map (e.g. white, uniform color, or the result from k-means).

The *albedo map* is estimated by minimizing the same cost with a small variant – we give a lower confidence to points with low shading. Also, a weighted local smoothing term is added based on the difference in intensity.

$$E'_{\text{template}}(\hat{\rho}) = \sum_{i \in \mathcal{V}} w_i^a \left\| \hat{\mathbf{I}}_i^{\text{diff}} - \hat{\rho}_i r(\mathbf{n}_i(\hat{\mathbf{S}})) \right\|_{\epsilon} \quad (13)$$

$$+ \sum_{i \in \mathcal{V}} \sum_{j \in \mathcal{N}_i} w_{ij}^{a'} \|\hat{\rho}_i - \hat{\rho}_j\|_2^2$$

where  $w_i^a = r(\mathbf{n}_i)$  is chosen to decrease the importance placed on regions of low shading and  $w_{ij}^{a'} = \exp\left(-\frac{\|\mathbf{I}_i - \mathbf{I}_j\|_2^2}{2\sigma_s^2}\right)$  to encourage points with similar appearance to share the same albedo.



**Fig. 5 Depth Fusion:** To illustrate that our approach to NRSfM can be fused with other depth cues, we show results from our method both with and without data from a depth camera. The results show a comparison between the results of Zollhofer et al. (2014) and our methods with and without depth data on a real face sequence taken from Zollhofer et al. (2014). Owing to the strong illumination effects, missing data and strong specularities, a direct comparison with Yu et al. (2015) was not possible, as quality of the reconstruction was very poor. In contrast, the results of our method using the same RGB input only (*Ours (no depth)*) provides good quality results. This justifies the need to reason jointly about shading, specularities and normals in the context of non-rigid tracking from RGB only, as we argue for in this paper.

## 8 Experimental Evaluation

We consider the experimental evaluation on two separate problems: (i) Evaluating our results when using only an RGB video sequence as input, and (ii) Using input from an RGB-D camera as input.

### 8.1 Video Input

#### 8.1.1 Experiments on sequences with ground truth 3D

We tested the proposed method on ground truth sequences that we generated using the public dataset of 3D face shapes

from Valgaerts et al. (2012), down-sampled ten times in order to reduce the runtime of our method. These 3D shapes were reconstructed by Valgaerts et al. (2012), using their high end stereo algorithm, from a real video sequence of an actor and were made publicly available. Using these 3D shapes as ground truth geometry in conjunction with the original video we render various ground truth sequences under different lighting conditions and surface properties.

We assign a constant albedo over time to each of the vertices of the mesh, which we estimated using the 3D ground truth shape associated with the first frame in a similar way as described in section 7. Using this albedo map, we render four different scenarios combining Lambertian or specular

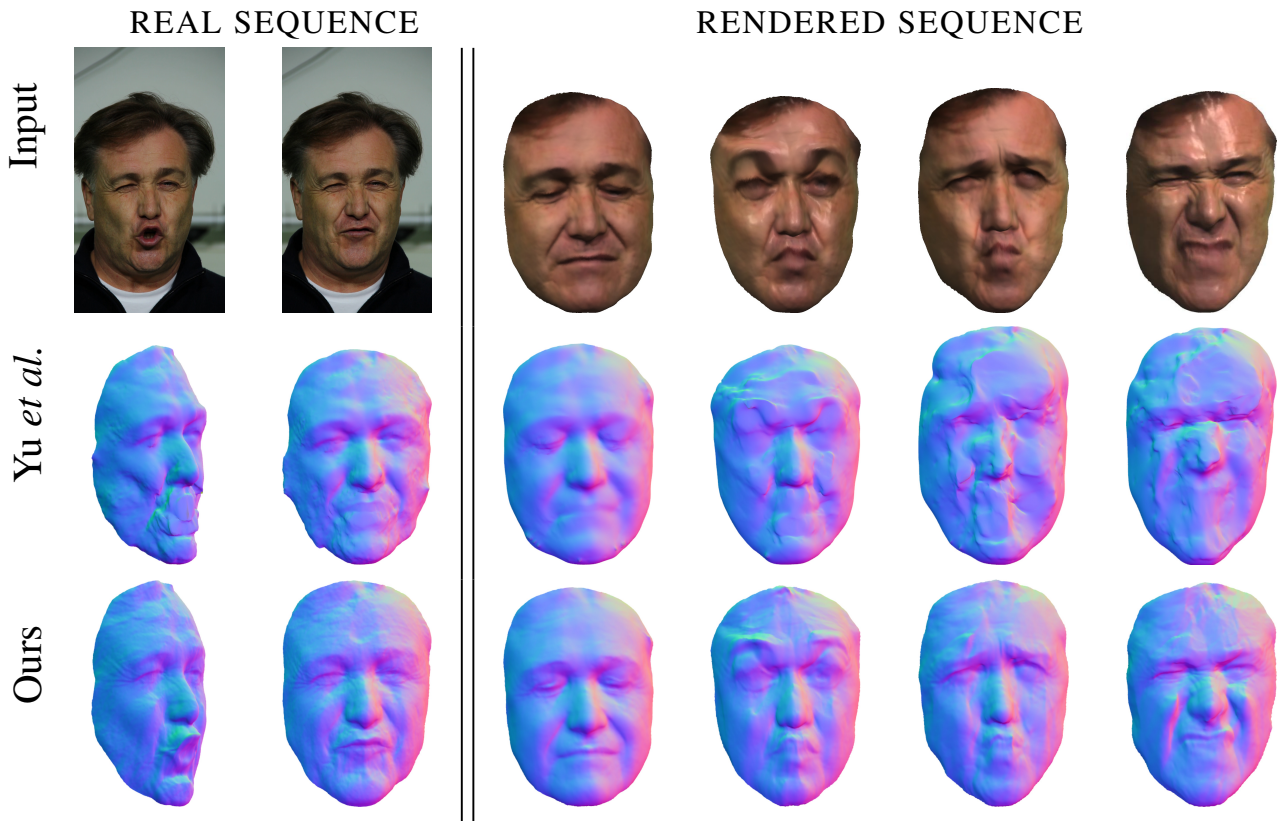


**Fig. 6** Best viewed in color: A qualitative comparison of our method against that of Yu et al. (2015), on (LEFT) the real-world sequence of Valgaerts et al. (2012) and (RIGHT) our four rendered sequences (from left to right: LF, SF, LC and SC).

surfaces on a scene lit by two white directional lights with constant or changing intensity. Thus, we have sequences with a perfect Lambertian surface with fixed (LF) or changing illumination (LC), and a specular surface with fixed (SF) or changing illumination (SC) (see figures 2 and 6). To test these ground truth sequences we use a coarse-to-fine pyramid with a template mesh of  $\sim 6,000$  vertices at the coarsest level and, for the finest level, one with the same amount of vertices as the ground truth ( $\sim 24,000$  vertices). We run our method on a computer with an Intel Core i7-5930K CPU, which takes around one minute to process each frame.

Table 1 shows the comparison results against the recent template-based method of Yu et al. (2015) using their publicly available code<sup>2</sup>. It can be seen that our proposed approach is significantly better in all four cases, both when we do and when we do not model specularities. We reduce the baseline error by a factor of 220%-260% when the specular component is not estimated and around 240%-280% when it is. It should also be noticed how estimating the specular component improves the results for pure Lambertian sequences. This is due to the fact that the estimated specularities are also compensating for the errors in the initially computed albedo. Figure 4 shows the decomposition of two

different input frames of the SC sequence (with a specular surface and changing illumination) into *albedo*, *shading*, *specularities*, *normals* and *illumination*. We show how our method can handle this challenging scenario with significant changes in intensity. Our results can be best appreciated by watching the accompanying video<sup>3</sup>.

### 8.1.2 Experiments on real sequences

We further evaluate qualitatively on real sequences: the original face from Valgaerts et al. (2012) (figure 6), the face from Yu et al. (2015) (figure 3), and new sequences of a hand deforming a ball (figure 9) and two child faces (figure 7). In the case the first sequence (figure 6), notice the improvement on the reconstructed deformation of the mouth thanks to our diffuse shading model while Yu et al. (2015) only able to recover a flat surface. We do not show a comparison with Yu et al. (2015) on the two sequences of the child faces (figure 7) as the reconstructions were of poor quality given the specularities and strong deformations.

<sup>3</sup> Please visit [http://www0.cs.ucl.ac.uk/staff/Qi.Liu/bmvcl6/better\\_together.html](http://www0.cs.ucl.ac.uk/staff/Qi.Liu/bmvcl6/better_together.html) to check video results and to access our publicly available code and datasets.

<sup>2</sup> <http://visual.cs.ucl.ac.uk/pubs/ddd/>

**Table 1** Comparison of different versions of our algorithm with Yu et al. (2015) on 4 different synthetic sequences. We report average RMS error (in mm) over all frames w.r.t. ground truth. The four experiments refer either to Lambertian (L) or Specular (S) surfaces with fixed (F) or changing (C) lighting. We also show a quantitative comparison between different versions of our own algorithm. Our results can be improved by joint refinement of all energy terms, and the use of depth maps. Note that joint refinement leads to a substantial increase in robustness, that can be seen not just in the better results but also in the slower rate of degradation, as we move to more challenging sequences. As expected, the use of RGB-D data as input gives a substantial improvement over RGB only.

	LF (mm)	SF (mm)	LC (mm)	SC (mm)
Yu et al. (2015)	7.29	7.93	9.18	9.28
Ours without specularities	2.91	3.28	3.50	4.21
Ours with specularities	2.73	2.89	3.42	3.84
Ours With Joint Refinement	2.71	2.80	3.11	3.01
Ours With Depth	1.73	1.79	1.71	1.81
Ours With Depth & Joint Refinement	1.64	1.74	1.72	1.77



**Fig. 7** Example reconstructions on real sequences with strong deformations.

### 8.1.3 Influence of the template quality

One important question is how much do the quality of our results depend upon high quality templates that we deform to track the object? Is our algorithm robust to small discrepan-

cies between the template and the ground-truth, or will small mistakes in the template propagate leading to drifting reconstructions? Figure 8 and table 2 show that our method exhibits robustness to small amounts of noise with the error being as likely to increase as to decrease as the template error increases. This can perhaps be attributed to the first frame of the ground-truth being used as a template in the synthetic sequence. The first frame is not a perfect example of the face at rest, that should have zero spatial smoothness costs (i.e. total-variation as defined in section 5.1.2, and ARAP as defined in section 5.1.3) associated with it, and small amount of noise have little impact on the quality of the solution.

Note that this experiment was conducted on the *real* sequence from Valgaerts et al. (2013). Although we generate the RMS errors with respect to the difference between our results and geometry given by the multi-camera reconstruction of Valgaerts et al. (2013), the reader should bear in mind that the 3D reconstruction given by Valgaerts et al. (2013) is not perfect ground-truth, just a better quality reconstruction produced using more data than our approach has access to.

## 8.2 Color and Depth Camera Input

To illustrate the versatility of our approach to non-rigid SfM and to show that it can also be combined with other important cues about 3D shape such as depth maps, we evaluate our method on the RGB-D face sequence of Zollhofer et al. (2014). As can be seen in figure 5, this is a highly challenging sequence that contains extreme changes in appearance due to both Lambertian shading and specular effects. As mentioned in section 2, these effects are so strong that Zollhofer et al. (2014) only makes uses of color in its frame-to-frame tracking, as the effects of shading and specularities are relatively constant over these short two frame subsequences. However, by correctly formulating our color term as a decomposition into variable lighting, specularities and consistent albedo, we are able to track using a frame-to-model ap-

**Table 2** Template noise: The pose and 3D estimation of shapes does not require perfect templates and in fact is robust to different levels of Gaussian noise in the template reconstruction. See section 8.1.3 for details.

Template noise	$\sigma = 0$	$\sigma = 0.001$	$\sigma = 0.005$	$\sigma = 0.008$	$\sigma = 0.01$
No joint optimization	3.1080	3.1339	3.1364	3.3118	3.5791
Joint optimization	3.0626	3.1081	3.1617	3.3012	3.5477

proach and reliably reconstruct from RGB input only even without using depth as a cue (see (*Ours (no depth)*) figure 5).

Unfortunately, the images used to build the 3D templates of Zollhofer et al. (2014) were no longer available at the time of writing, and we were unable to estimate the albedo of the template provided. Instead, we took the reconstruction in the first frame, colored using the image data, as our template.

Zollhofer et al. (2014) treats the output of an infra-red stereo camera rig as a noisy depth mask and makes use of temporal consistency, frame-to-frame color consistency and shape-based regularization to track and denoise the output. For a fair comparison, we also take the noisy depth map as a direct input and encourage agreement between our reconstruction and the depth map using the additional cost of (11). Qualitative results can be seen in figure 5.

We also evaluated the quantitative impact of using depth data on the reconstructions conducted with synthetic sequences. Table 1 shows that the use of depth data gives a substantial improvement over RGB only.

## Acknowledgments

This work was partly supported by the SecondHands project, funded from the European Unions Horizon 2020 Research and Innovation programme under grant agreement No 643950. Qi Liu-Yin was funded by a UCL/Microsoft Research studentship. Chris Russell was partially supported by The Alan Turing Institute under the EPSRC grant EP/N510129/1.

## 9 Conclusion

We have presented a principled approach to jointly reason about non-rigid structure from motion and shape-from-shading, and provided strong empiric evidence that it is required to avoid systematic tracking failures, and that it significantly improves the reconstruction quality of fine semantic details. Although, we focused upon the challenging problem of reconstruction from a single RGB camera, we have also shown that joint reasoning about the motions of deformable objects and shape-from-shading can readily be applied to RGB-D and multi-camera based approaches, and the increased robustness and detailed reconstructions it brings is likely to be of use to the wider community.

## References

- Agarwal S, Mierle K, et al. (2012) Ceres solver. <http://ceres-solver.org>
- Basri R, Jacobs DW (2003) Lambertian reflectance and linear subspaces. *IEEE Trans Pattern Anal Mach Intell* 25(2):218–233
- Beeler T, Bradley D, Zimmer H, Gross M (2012) Improved reconstruction of deforming surfaces by cancelling ambient occlusion. In: 12th European Conference on Computer Vision, Springer Berlin Heidelberg, Berlin, Heidelberg, pp 30–43
- Campbell ND, Vogiatzis G, Hernández C, Cipolla R (2008) Using multiple hypotheses to improve depth-maps for multi-view stereo. In: *ECCV*
- Dou M, Taylor J, Fuchs H, Fitzgibbon A, Izadi S (2015) 3d scanning deformable objects with a single rgbd sensor. In: *The IEEE Conference on Computer Vision and Pattern Recognition (CVPR)*
- El RO, Hershkovitz R, Wetzler A, Rosman G, Bruckstein A, Kimmel R (2016) Real-time depth refinement for specular objects. In: *IEEE Conference on Computer Vision and Pattern Recognition (CVPR)*
- Garrido P, Valgaerts L, Wu C, Theobalt C (2013) Reconstructing detailed dynamic face geometry from monocular video. In: *ACM Trans. Graph. (Proc. SIGGRAPH Asia)*
- Hernández C, Vogiatzis G, Cipolla R (2007) Probabilistic visibility for multi-view stereo. In: *CVPR*
- Kemelmacher-Shlizerman I, Seitz SM (2011) Face reconstruction in the wild. In: *Computer Vision (ICCV), 2011 IEEE International Conference on, IEEE*, pp 1746–1753
- Klein G, Murray D (2007) Parallel tracking and mapping for small AR workspaces. In: *ISMAR*
- Malti A, Bartoli A, Collins T (2012) Template-based conformal shape-from-motion-and-shading for laparoscopy. In: *Information Processing in Computer-Assisted Interventions*
- Newcombe R, Lovegrove S, Davison A (2011) DTAM: Dense Tracking and Mapping in Real-Time. In: *ICCV*
- Newcombe R, Fox D, Seitz S (2015) Dynamicfusion: Reconstruction and tracking of non-rigid scenes in real-time. In: *CVPR*
- Nishino K, Zhang Z, Ikeuchi K (2001) Determining reflectance parameters and illumination distribution from a sparse set of images for view-dependent image synthe-

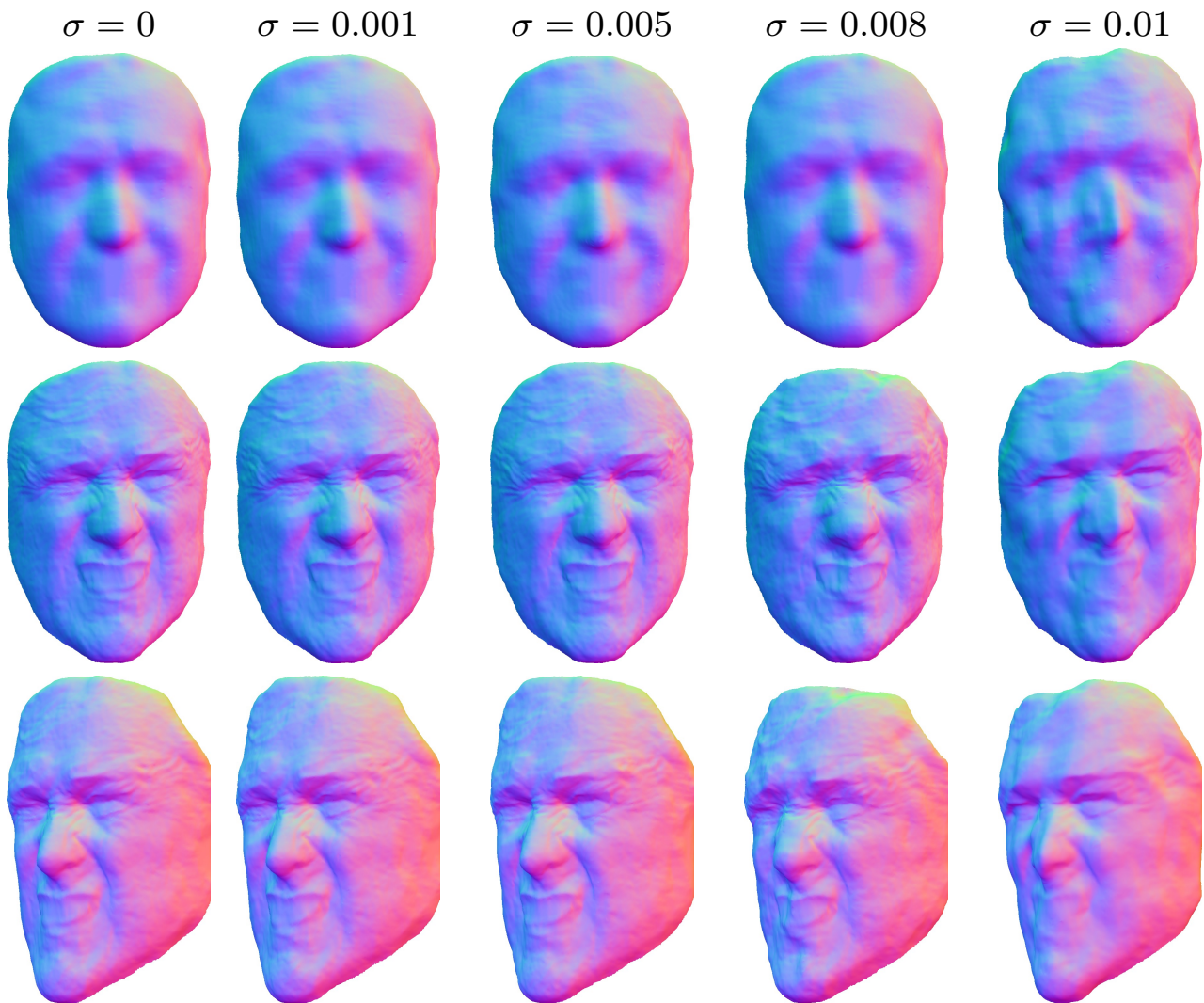


**Fig. 8** Best viewed in color: A qualitative comparison of our tracking results on real sequence using different templates, shown in the top row, with different levels of Gaussian noise. The second and third row show the tracking results of one selected frame.

- sis. In: Computer Vision, 2001. ICCV 2001. Proceedings. Eighth IEEE International Conference on, IEEE, vol 1, pp 599–606
- Or El R, Rosman G, Wetzler A, Kimmel R, Bruckstein AM (2015) Rgb-d-fusion: Real-time high precision depth recovery. In: The IEEE Conference on Computer Vision and Pattern Recognition (CVPR)
- Sorkine O, Alexa M (2007) As-rigid-as-possible surface modeling. In: Proceedings of the Fifth Eurographics Symposium on Geometry Processing, SGP '07
- Sundaram N, Brox T, Keutner K (2010) Dense point trajectories by gpu-accelerated large displacement optical flow. In: ECCV
- Suwajanakorn S, Kemelmacher-Shlizerman I, Seitz SM (2014) Total moving face reconstruction. In: ECCV
- Valgaerts L, Wu C, Bruhn A, Seidel HP, Theobalt C (2012) Lightweight binocular facial performance capture under uncontrolled lighting. In: ACM Transactions on Graphics (Proceedings of SIGGRAPH Asia 2012), vol 31, pp 187:1–187:11
- Valgaerts L, Bruhn A, Seidel HP, Theobalt C (2013) Lightweight binocular facial performance capture under uncontrolled lighting. SIGGRAPH
- Varol A, Shaji A, Salzmann M, Fua P (2012) Monocular 3d reconstruction of locally textured surfaces. Pattern Analysis and Machine Intelligence, IEEE Transactions on 34(6):1118–1130
- Vogiatzis G, Hernández C, Torr P, Cipolla R (2007) Multi-view stereo via volumetric graph-cuts and occlusion robust photo-consistency. PAMI
- Wood DN, Azuma DI, Aldinger K, Curless B, Duchamp T, Salesin DH, Stuetzle W (2000) Surface light fields for 3d photography. In: Proceedings of the 27th annual conference on Computer graphics and interactive techniques,

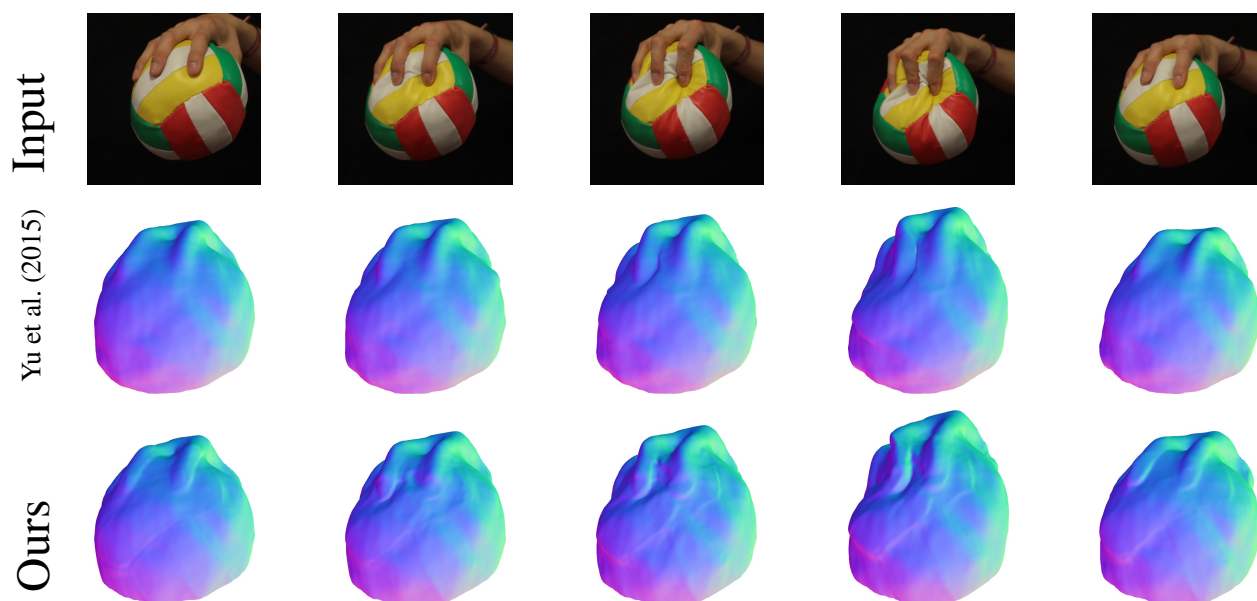


Fig. 9 Comparison between the results of Yu et al. (2015) and our method on a real sequence of a hand holding and deforming a ball.

ACM Press/Addison-Wesley Publishing Co., pp 287–296

Wu C (2011) Visualsfm: A visual structure from motion system. <http://ccwu.me/vsfm/>

Xu Y, Roy-Chowdhury AK (2005) Integrating the effects of motion, illumination and structure in video sequences. In: Computer Vision, 2005. ICCV 2005. Tenth IEEE International Conference on, IEEE, vol 2, pp 1675–1682

Yu LF, Yeung SK, Tai YW, Lin S (2013) Shading-based shape refinement of rgb-d images. In: Proceedings of the IEEE Conference on Computer Vision and Pattern Recognition, pp 1415–1422

Yu R, Russell C, Campbell N, Agapito L (2015) Direct, dense, and deformable: Non-rigid 3d reconstruction from rgb video. ICCV

Zollhofer M, Niessner M, Izadi S, Rehmann C, Zach C, Fisher M, Wu C, Fitzgibbon A, Loop C, Theobalt C, Stamminger M (2014) Real-time non-rigid reconstruction using an rgb-d camera. SIGGRAPH